Int. J. Heat Mass Transfer. Vol. 27, No. 11, pp. 2085–2093, 1984
Printed in Great Britain

0017–9310/84 $3.00 + 0.00

Radiant heat transfer through the cover gas of a sodium-cooled fast reactor

J. S. TRUELOVE
Department of Chemical Engineering, University of Newcastle, NSW 2308, Australia

(*Received* 7 *June* 1983 *and in revised form* 8 *March* 1984)

Abstract—A simple model of radiant heat transfer through the cover gas in a sodium-cooled fast reactor is presented. The cover gas medium is assumed to consist of a cloud of sodium droplets suspended in a transparent gas. The radiative properties of the droplet cloud—absorption and scattering efficiencies and scattering phase function—are calculated using the Mie theory of electromagnetic scattering with optical properties predicted by the classical electron theory of metals. Radiative transfer through the cover gas is calculated rigorously using the discrete ordinate method and compared with the results obtained by the isotropic scaling and Eddington approximations. Numerical results of the model are presented and used to estimate the effect of droplet scattering on heat transfer through the fast reactor cover gas.

1. INTRODUCTION

PRELIMINARY calculations by Clement and Hawtin [1] of heat and mass transfer through the cover gas in a sodium-cooled fast reactor suggest that thermal radiation is the dominant mechanism for heat transfer from the pool to the roof. In analysing the radiative transfer, Clement and Hawtin assumed the cover gas medium to be transparent. However, theoretical [1] and experimental [2] studies have shown that sodium vapour condenses in the cover gas cavity with the formation of a cloud of sodium droplets suspended in the cover gas. When the droplets are present in a significant concentration then consideration must be given to the effect of radiation scattering and absorption. The purpose of this work is to examine the influence of the droplet cloud on radiative heat transfer through the cover gas.

In the present work, the analysis of Clement and Hawtin is extended to incorporate the interaction of radiation with a cloud of sodium droplets suspended in the cover gas. The physical model of the cover gas cavity is described briefly in Section 2. The calculation of the radiative properties of the cloud of sodium droplets is presented in Section 3. The analysis of heat and mass transfer through the cover gas is given in Section 4 with details of the radiant heat transfer calculation in Section 5. Finally, the effect of the droplet cloud on heat transfer through the fast reactor cover gas is estimated in Section 6.

2. PHYSICAL MODEL AND ASSUMPTIONS

Following Clement and Hawtin [1], the cover gas cavity is modelled as an infinite planar medium bounded by two horizontal plane surfaces. The plane surfaces, representing the sodium pool and the roof of the vessel, are at prescribed temperatures, the lower surface (sodium pool) being at the higher temperature.

The cover gas medium consists of a cloud of small sodium droplets suspended in an inert gas (argon) saturated with sodium vapour. The mass fraction of sodium vapour in the gas/vapour mixture is small ($\lesssim 10^{-2}$) and the properties of the mixture are taken to be those of the inert gas. The sodium droplets typically have diameters less than 20 μm [2] and are presumed to be at the same temperature as the surrounding gas and distributed uniformly throughout the cover gas cavity. The limited data on sodium aerosols [2, 3] suggest that the droplet mass fraction is small ($\lesssim 10^{-1}$).

The buoyancy-driven flow within the cavity is turbulent (Rayleigh number about 2×10^9) and the medium is presumed to be at uniform temperature, although in practice there will be large temperature gradients in narrow thermal boundary layers near the pool and the roof. The existence of a uniform-temperature core region is supported by experimental [4, 5] and theoretical [6] investigations of thermal convection in horizontal layers of air heated from below, and also fluid layers heated volumetrically [7]. The volumetrically heated layer is pertinent to the present investigation because condensation of sodium vapour generates heat within the cover gas medium. At the above mentioned Rayleigh number, the thermal boundary layer occupies less than 1% of the width of the heated layer [4]. Measured fluid velocities [8] are consistent with a turbulent structure in which the dominant eddies extend across the full width of the layer. Estimated vertical flow velocities in the cover gas cavity (~ 1 m s^{-1}) are high enough to hold the sodium droplets in suspension against the settling force of gravity.

The transfer of heat from the pool to the roof by natural convection, evaporation and condensation is expressed simply as the product of a heat-transfer coefficient and an enthalpy difference. The analogy between heat and mass transfer is invoked to estimate the mass fluxes of sodium vapour due to evaporation and condensation. The heat-transfer coefficient is assumed to be the same as that in the absence of mass

NOMENCLATURE

a_n	expansion coefficient, equation (22)
c	velocity of light in vacuo, 3×10^8 m s^{-1}
C	mass concentration [kg m^{-3}]
C_p	specific heat [J kg^{-1} K^{-1}]
$\overline{DS}$	droplet cloud-to-surface configuration factor
e	electron charge, 1.6×10^{-19} C
h	specific enthalpy [J kg^{-1}]
I	total radiation intensity [W m^{-2} sr^{-1}]
$I_{b,\lambda}$	blackbody spectral intensity [W m^{-3} sr^{-1}]
k	imaginary part of complex refractive index
K_a	absorption coefficient [m^{-1}]
K_s	scattering coefficient [m^{-1}]
L	latent heat [J kg^{-1}]
m	mass fraction [kg kg^{-1}]
$\mathbf{m}$	complex refractive index
m_e	electron mass, 9.11×10^{-31} kg
n	real part of complex refractive index
$n(r)$	droplet size distribution [m^{-4}]
N	number density of droplets in cloud [m^{-3}]
N_e	number density of conduction electrons [m^{-3}]
p	phase function
P_n	Legendre polynomial of degree n
q	heat flux [W m^{-2}]
Q	efficiency factor
r	radius of droplet [m]
r_g	mean geometric radius [m]
$\bar{r}_{32}$	Sauter mean radius [m]
$\overline{SS}$	surface-to-surface configuration factor
T	temperature [K]
x	distance [m].

Greek symbols

α	heat-transfer coefficient [kg m^{-2} s^{-1}]
γ	damping frequency [rad s^{-1}]
ε	emissivity of surface
ε_0	permittivity constant in vacuo, 8.84×10^{-12} F m^{-1}
λ	wavelength [m]
μ	direction cosine
μ_0	cosine of scattering angle
$\langle\mu_0\rangle$	asymmetry
ν	frequency [rad s^{-1}]
ρ_d	droplet density [kg m^{-3}]
σ_0	electrical conductivity [Ω^{-1} m^{-1}]
σ	Stefan–Boltzmann constant, 5.67×10^{-8} W m^{-2} K^{-4}
σ_g	standard geometric deviation
τ	optical depth
τ_0	optical thickness
ω	single-scatter albedo.

Subscripts

a	absorption
con	convection
d	droplet
g	gas
r	radius
rad	radiation
s	scattering
λ	spectral
1(2)	surface 1(2).

Superscript

*	scaled (to isotropic).

transfer. These assumptions are justified because the mass flux of vapour is small ($\lesssim10^{-4}$ kg m^{-2} s^{-1}), and consequently the boundary layers which provide the principal resistance to heat transfer, are not significantly perturbed. Heat and mass transfer by natural convection, evaporation and condensation is discussed in depth elsewhere [1, 9]. A detailed model for these processes, such as that presented in ref. [1], is not warranted in the present investigation where the emphasis is on heat transfer by radiation.

The sodium covered surfaces bounding the medium are assumed to be radiatively grey and to emit and reflect radiation diffusely. The inert gas and sodium vapour in the medium are transparent, while the sodium droplets absorb, emit and anisotropically scatter thermal radiation. The absorption and emission of radiation by metals such as sodium is small and therefore the process of heat transfer by radiation is not strongly coupled to the other heat transfer processes.

3. RADIATIVE PROPERTIES OF SODIUM DROPLET CLOUD

3.1. *Optical constants*

The response of a material to an applied electromagnetic field, such as infrared radiation, can be described by the optical constants n and k which are the real and imaginary parts of the complex refractive index $\mathbf{m}$ ($=n-ik$), respectively. For alkali metals such as sodium, the classical electron theory of metals yields the following dispersion equations relating the optical constants at frequencies in the infrared to the electronic properties of the material [10]

$$n^2-k^2=1-\frac{N_e e^2}{\varepsilon_0 m_e(\nu^2+\gamma^2)} \tag{1}$$

$$2nk=\frac{N_e e^2\gamma}{\varepsilon_0 m_e\nu(\nu^2+\gamma^2)} \tag{2}$$

where N_e is the number of conduction electrons per unit

volume, e and m_e are the electronic charge and mass, respectively, ε_0 is the permittivity constant in vacuo, γ is a damping frequency and v is the angular frequency of the radiation (related to the wavelength in vacuo, λ, by $v = 2\pi c/\lambda$). The damping frequency is assumed to be independent of v and is obtained from the observed zero-frequency (direct-current) electrical conductivity σ_0 as

$$\gamma = \frac{N_e e^2}{m_e \sigma_0}. \tag{3}$$

Typical values of the electronic properties (N_e and σ_0) of sodium at room temperature are [11]

$$N_e = 2.5 \times 10^{28}\ \mathrm{m}^{-3}$$

$$\sigma_0 = 2.1 \times 10^7\ \Omega^{-1}\ \mathrm{m}^{-1}.$$

Figure 1 shows the calculated infrared optical constants of sodium at temperatures of 290, 670 and 870 K, the last two of which are typical of the temperatures encountered in the fast reactor cover gas cavity. The variation of n and k with temperature results from the temperature dependence of N_e (proportional to density) and σ_0. At the high temperatures sodium is in the liquid state (melting point 371 K). The results indicate that both n and k increase significantly with increasing wavelength, a feature which is characteristic of metals. In the near infrared ($\lambda \approx 1\ \mu$m), k is more than an order of magnitude greater than n, while in the far infrared ($\lambda \geqslant 20\ \mu$m), n and k asymptotically approach the same value. Also shown in Fig. 1 are measurements

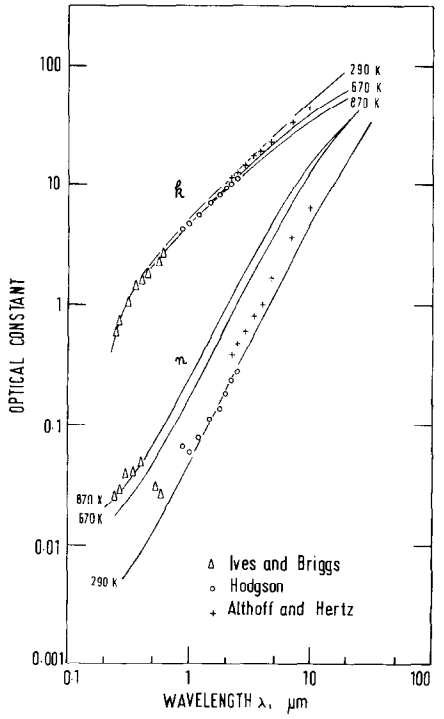

FIG. 1. Optical constants for sodium. The data are for a temperature of 290 K: △, Ives and Briggs [12]; ○, Hodgson [13]; +, Althoff and Hertz [14].

[12–14] of the optical constants at room temperature. For the range of wavelengths of interest in the present study, namely 2–20 μm, the calculated and measured values of n and k are in good agreement. The discrepancy between the calculated and measured values of n at wavelengths between 2.5 and 10 μm is attributable to a systematic error in the experimental data: Althoff and Hertz [14] report that their measured optical constants are imprecise due to impurities in the surface of the sodium sample and that the value of σ_0 inferred from the data is in error by 30%. The discrepancy at low wavelengths is expected because the classical electron theory of metals is known to break down at wavelengths in the visible region.

The success of the classical electron theory of metals in calculating the infrared optical constants of sodium at room temperature suggests that the predictions at the higher temperatures should be reliable.

3.2. *Radiative properties for a single droplet*

The efficiencies for absorption and scattering of radiation by a spherical droplet with complex refractive index $\mathbf{m}$ can be calculated from the Mie equations [15]. Here, the absorption and scattering efficiencies are denoted by $Q_{a,\lambda,r}$ and $Q_{s,\lambda,r}$, respectively, where λ is the wavelength of the incident radiation in the medium surrounding the droplet and r is the radius of the droplet. The angular distribution of the scattered radiation, which can also be calculated from the Mie equations, is described by the scattering phase function, denoted here by $p_{\lambda,r}(\mu_0)$ where μ_0 is the cosine of the scattering angle. The Mie equations and associated computational methods are given in detail elsewhere [15, 16].

3.3. *Radiative properties for a cloud of droplets*

For a cloud of spherical droplets in which the individual droplets are well separated the absorption and scattering coefficients and the phase function are obtained as the sum of the individual droplet contributions. Thus, for a cloud with droplet size distribution function $n(r)$, the scattering coefficient is given by

$$K_{s,\lambda} = \int_0^\infty n(r)\pi r^2 Q_{s,\lambda,r}\ \mathrm{d}r. \tag{4}$$

This expression can be rewritten as

$$K_{s,\lambda} = \frac{3Q_{s,\lambda}C}{4\rho_d \bar{r}_{32}} \tag{5}$$

where C is the mass concentration of droplets in the cloud, ρ_d is the droplet density, $\bar{r}_{32}$ ($= \langle r^3\rangle/\langle r^2\rangle$) is the Sauter mean radius for the droplet distribution and $Q_{s,\lambda}$ is the cloud scattering efficiency given by

$$Q_{s,\lambda} = \frac{\int_0^\infty n(r)\pi r^2 Q_{s,\lambda,r}\ \mathrm{d}r}{\int_0^\infty n(r)\pi r^2\ \mathrm{d}r}. \tag{6}$$

Similarly, the absorption coefficient, $K_{a,\lambda}$, and cloud absorption efficiency, $Q_{a,\lambda}$, are given by equations (4)–(6) with the subscript 's' replaced by 'a'. The cloud phase function is given by

$$p_\lambda(\mu_0) = \frac{1}{K_{s,\lambda}} \int_0^\infty n(r)\pi r^2 Q_{s,\lambda,r} p_{\lambda,r}(\mu_0)\, dr. \quad (7)$$

The asymmetry, or forwardness of scatter, $\langle \mu_0 \rangle_\lambda$, is defined as

$$\langle \mu_0 \rangle_\lambda = \frac{1}{2} \int_{-1}^{1} p_\lambda(\mu_0)\mu_0\, d\mu_0. \quad (8)$$

The sparse experimental data relevant to sodium droplet clouds in the fast reactor suggest that the droplets have radii in the range 0.5–10 μm [2] and that, to a first approximation, the cloud has a log-normal size distribution [3]. Thus, the droplet size distribution function is taken to be

$$n(r) = \frac{N}{r\sqrt{(2\pi)}\ln \sigma_g} e^{-1/2\left(\frac{\ln (r/r_g)}{\ln \sigma_g}\right)^2} \quad (9)$$

where N is the number density of droplets in the cloud, r_g is the mean geometric radius and σ_g is the standard geometric deviation.

Six typical size distributions, the parameters of which are given in Table 1, have been examined. The six distributions were chosen so that most of the droplets have radii within the observed range. The maximum value of σ_g (= 2.0) corresponds to about a 30-fold range of radius. Furthermore, the parameters were chosen so that several of the distributions have the same Sauter mean radius ($\bar{r}_{32}$) but differ in all other respects.

Figure 2 shows the calculated efficiencies for absorption and scattering of radiation by the six sodium droplet clouds at a temperature of 770 K. As expected, the cloud efficiencies are relatively smooth functions of wavelength and do not exhibit the oscillations characteristic of single droplet efficiencies. It can be seen that the efficiency factors for droplet clouds having the same Sauter mean radius are very similar. This feature of cloud efficiencies—that the mean efficiencies for polydispersions depend primarily on the Sauter mean size and only weakly on the detailed shape of the size distribution function—has also been reported for dielectric spheres [17, 18]. It is convenient to characterize the cloud properties in terms of the mean droplet size parameter for the cloud, defined as

Table 1. Size parameters and total radiative properties for the six typical droplet clouds

Property	1	2	3	4	5	6
r_g (μm)	1.18	1.38	2.05	1.62	2.40	3.56
σ_g	1.50	1.76	1.50	2.00	1.76	1.50
$\bar{r}_{32}$ (μm)	1.78	3.09	3.09	5.37	5.37	5.37
ω	0.965	0.968	0.969	0.971	0.971	0.972
$\langle \mu_0 \rangle$	0.231	0.333	0.353	0.400	0.420	0.440

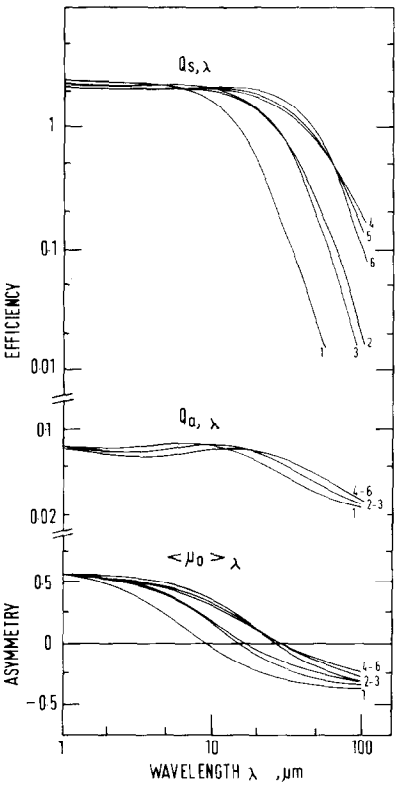

FIG. 2. Efficiencies and asymmetry of sodium droplet clouds at a temperature of 770 K.

$2\pi\bar{r}_{32}/\lambda$. When the size parameter is greater than unity, the cloud efficiencies are relatively constant—approximately 0.07 and 2.0 for absorption and scattering, respectively. Conversely, when the size parameter is less than unity, the absorption and scattering efficiencies decrease with decreasing size parameter, and are approximately proportional to the first and fourth powers of the size parameter, respectively.

Also shown in Fig. 2 is the asymmetry for each of the six cloud functions. Once again, it can be seen that the asymmetries for clouds having the same Sauter mean radius are similar. The scattered radiation is forward or backward directed ($\langle \mu_0 \rangle_\lambda$ greater or less than zero) depending upon whether the size parameter is greater or less than unity.

The efficiencies and asymmetry are essentially independent of the droplet temperature within the range 670–870 K, due to the weak dependence of **m** on temperature as shown in Fig. 1.

The absorption and scattering coefficients for the droplet cloud are obtained from the cloud efficiencies using equation (5). Because the cloud efficiencies are primarily dependent on the Sauter mean radius of the droplet cloud, it follows from equation (5) that, for a cloud with a given mass concentration of droplets, the absorption and scattering coefficients are also primarily dependent on the Sauter mean radius.

3.4. *Total radiative properties*

The analysis of radiant heat transfer is greatly simplified by using wavelength-averaged, or total, radiative properties. For the range of temperatures encountered in the fast reactor cover gas cavity (670–870 K), 95% of the thermal radiation lies at wavelengths in the range 2–20 μm with the maximum in the spectral distribution at about 4 μm. From Fig. 2 it is clear that within this range of wavelengths the variation of the efficiencies with wavelength is not large.

The wavelength-averaged scattering efficiency is defined by

$$Q_s = \frac{\int_0^\infty Q_{s,\lambda} I_{b,\lambda}\, d\lambda}{\int_0^\infty I_{b,\lambda}\, d\lambda} \tag{10}$$

where $I_{b,\lambda}$ is the black-body spectral intensity at the source temperature of the radiation. The wavelength-averaged absorption efficiency, Q_a, is defined by the same equation with the subscript 's' replaced by 'a'.

For the six sodium droplet clouds, the wavelength-averaged efficiencies calculated according to equation (10) are essentially independent of the radiation source temperature within the range 670–870 K. Furthermore, the total cloud efficiencies calculated according to equation (10) are only weakly dependent on both the shape of the size distribution and the mean radius of the droplets in the cloud. The average values of the efficiencies for the six clouds are

$$Q_a = 0.068 \pm 0.005$$

$$Q_s = 2.08 \pm 0.08.$$

The single-scatter albedo, $\omega (= Q_s/(Q_a + Q_s))$, calculated from the individual values of the efficiencies is

$$\omega = 0.968 \pm 0.003.$$

The wavelength-averaged absorption and scattering coefficients, K_a and K_s, are obtained from Q_a and Q_s using expressions similar to that given by equation (5).

The asymmetry of the wavelength-averaged phase function defined by

$$p(\mu_0) = \frac{\int_0^\infty p_\lambda(\mu_0) Q_{s,\lambda} I_{b,\lambda}\, d\lambda}{Q_s \int_0^\infty I_{b,\lambda}\, d\lambda} \tag{11}$$

is also essentially independent of source temperature, and increases slowly with increasing Sauter mean radius of the droplet cloud. For all six droplet clouds the scattering is forward directed ($\langle \mu_0 \rangle$ greater than zero).

The total radiative properties for the six sodium droplet clouds are summarized in Table 1.

4. HEAT TRANSFER IN CAVITY

With the assumptions given in Section 2 above, the net heat flux at the roof of the cavity (surface 2) due to convection and condensation is given by

$$q_{2,con} = \alpha_2 (h_g - h_2) \tag{12}$$

where α is the heat-transfer coefficient (based on enthalpy difference) and h is the specific enthalpy (sensible plus latent heat) of the gas–vapour mixture defined by

$$h = \int^T C_p\, dT + Lm \tag{13}$$

where C_p is the specific heat of the gas–vapour mixture, L is the latent heat of evaporation of sodium and m is the mass fraction of sodium vapour in the mixture. The subscripts g and 2 denote values at the temperature of the medium and surface 2, respectively. The mass fraction of sodium vapour in the mixture is taken as the saturation mass fraction at the temperature of the mixture. Use of the composite variable h, rather than separate variables T and m, enables heat transfer by convection and condensation to be described by a single equation. Furthermore, the composite variable h obeys a conservation equation of exactly the same form as that governing heat transfer in a non-condensing environment [19], and therefore the heat-transfer coefficient α can be estimated from Nusselt number correlations for turbulent convective heat transfer in the absence of condensation. It is implicit in the present formulation of heat and mass transfer that the Lewis number of the mixture is unity. For sodium/argon mixtures with a low mass fraction of sodium vapour the Lewis number does not deviate significantly from unity [9].

The net radiation heat flux at the roof surface can be written as [20]

$$q_{2,rad} = \overline{S_1 S_2}\sigma(T_1^4 - T_2^4) + \overline{DS_2}\sigma(T_d^4 - T_2^4) \tag{14}$$

where σ is the Stefan–Boltzmann constant, T is the temperature—subscripted 1, 2 and d for the lower surface (pool), upper surface (roof) and droplet-laden medium, respectively—and $\overline{S_1 S_2}$ and $\overline{DS_2}$ are configuration factors for radiative transfer from surface 1 to surface 2 and from the droplet-laden medium to surface 2, respectively. In the terminology of Hottel and Sarofim [20], $\overline{S_1 S_2}$ and $\overline{DS_2}$ are total exchange areas per unit area of the bounding surfaces. It is implicit in the formulation of equation (14) that wavelength-averaged radiative properties are employed in the calculation of the configuration factors.

The total heat flux at the roof, obtained by summing the contributions due to natural convection, condensation and radiation, is given by

$$q_2 = \overline{S_1 S_2}\sigma(T_1^4 - T_2^4) + \overline{DS_2}\sigma(T_d^4 - T_2^4) + \alpha_2 (h_g - h_2). \tag{15}$$

The expression for the total heat flux at the roof contains the unknown temperature of the medium. This may be eliminated by combining equation (15) with the equation obtained by formulating a heat

balance on the gas–vapour–droplet medium, namely

$$\overline{DS_1}\sigma(T_d^4 - T_1^4) + \overline{DS_2}\sigma(T_d^4 - T_2^4) + \alpha_1(h_g - h_1) + \alpha_2(h_g - h_2) = 0 \quad (16)$$

where the small sensible heat transfer associated with droplet deposition at the bounding surfaces is neglected. The heat-transfer coefficients at the two surfaces cannot be very different because the mass flux of sodium vapour at each surface is small and does not perturb the turbulent boundary layer significantly. Therefore, the coefficients α_1 and α_2 are presumed to be the same and denoted by α. The configuration factors $\overline{DS_1}$ and $\overline{DS_2}$ are the same because the two surfaces have the same emissivity, both being coated with sodium. Combining equations (15) and (16) gives

$$q_2 = (\overline{S_1S_2} + \tfrac{1}{2}\overline{DS_2})\sigma(T_1^4 - T_2^4) + \tfrac{1}{2}\alpha(h_1 - h_2). \quad (17)$$

The determination of the configuration factors for radiative transfer is described in the next section.

5. CONFIGURATION FACTORS FOR RADIATION

5.1. *Radiative transfer equation*

The equation for radiative transfer in a planar medium which absorbs, emits and scatters anisotropically can be written as [21]

$$\mu\frac{\partial I}{\partial \tau}(\tau,\mu) + I(\tau,\mu) = (1-\omega)\frac{\sigma T^4}{\pi} + \tfrac{1}{2}\omega\int_{-1}^{1} p(\mu,\mu')I(\tau,\mu')\,d\mu' \quad (18)$$

where $I(\tau,\mu)$ is the total (wavelength-integrated) intensity at optical depth τ in the μ direction. Here the optical depth coordinate is defined as

$$\tau = (K_a + K_s)x \quad (19)$$

where x is the geometric distance from surface 1 measured normal to the surface, and K_a and K_s are the total absorption and scattering coefficients of the medium. The optical thickness of the medium is denoted by τ_0. The single-scatter albedo, ω, is defined by

$$\omega = \frac{K_s}{K_a + K_s}. \quad (20)$$

Azimuthal symmetry is assumed and μ is the cosine of the polar angle measured from the positive x-direction. The scattering phase function is given by its Legendre expansion as

$$p(\mu,\mu') = 1 + \sum_{n=1}^{\infty} a_n P_n(\mu)P_n(\mu') \quad (21)$$

where $P_n(\mu)$ is the Legendre polynomial of degree n, and the expansion coefficients a_n are given by

$$a_n = \frac{2n+1}{2}\int_{-1}^{1} p(\mu_0)P_n(\mu_0)\,d\mu_0. \quad (22)$$

Boundary conditions for the transfer equation, appropriate to diffuse emission and reflection of radiation, are imposed at the bounding surfaces located at $\tau = 0$ (surface 1) and τ_0 (surface 2).

The configuration factors are obtained from the net radiative flux, defined by

$$q(\tau) = 2\pi\int_{-1}^{1} I(\tau,\mu)\mu\,d\mu \quad (23)$$

evaluated for the following specific conditions

$\overline{S_1S_2} = q(\tau_0)$ for conditions

$$\sigma T_1^4 = 1, \quad T_2 = T = 0 \quad (24)$$

$\overline{DS_2} = q(\tau_0)$ for conditions

$$T_1 = T_2 = 0, \quad \sigma T^4 = 1. \quad (25)$$

The combination of configuration factors in the expression for the total heat flux at surface 2 [equation (17)] is given by

$\overline{S_1S_2} + \frac{1}{2}\overline{DS_2} = q(\tau_0)$ for conditions

$$\sigma T_1^4 = 1, \quad \sigma T^4 = 0.5, \quad T_2 = 0. \quad (26)$$

5.2. *Solution of transfer equation*

The integro-differential transfer equation (18) may be solved numerically by the well-known discrete-ordinate, or quadrature, method [21]. The application of the method in a plane-parallel geometry is described in detail by Love and Grosh [22]. In the present work, a double Gaussian quadrature of order 10 (DS_{10}) was used for the angle integrations. The spatial integration was performed using standard finite-difference techniques. The final solution of the coupled equations for the intensity field was obtained iteratively, with a convergence criterion of $10^{-3}\%$ change between two consecutive iterations. The coefficients in the series expansion of the phase function were calculated by numerical integration of equation (22). The series expansion of the phase function was truncated after N significant terms, with the criterion $a_{N+1} < 10^{-2}$. For the six cloud phase functions examined in this work the value of N was typically less than 80.

5.3. *Approximate solution of transfer equation*

5.3.1. *Isotropic scaling.* The calculation of angle-integrated quantities, such as the net radiative heat flux, does not require precise detail in the scattering phase function. Consequently, when only angle-integrated quantities are of interest, the problem of forward-directed anisotropic scattering can be greatly simplified by approximating the exact phase function by the sum of a forward delta function and an isotropic scattering function [23]. The strength of the delta function is chosen to ensure the correct asymmetry [24], which is related to the coefficient a_1 in the series expansion of the exact phase function by $\langle\mu_0\rangle = a_1/3$. With this approximation, the anisotropic scattering problem is scaled to isotropic with the optical depth, single-scatter

albedo and phase function transformed according to

$$\tau^* = (1-\omega\langle\mu_0\rangle)\tau \quad (27)$$

$$\omega^* = \omega(1-\langle\mu_0\rangle)/(1-\omega\langle\mu_0\rangle) \quad (28)$$

$$p^*(\mu,\mu') = 1 \quad (29)$$

where the starred quantities refer to the isotropic problem. The isotropic scattering problem is amenable to a range of powerful analytic techniques [21, 25].

The scaling equations (27)–(29) ensure that the isotropic and anisotropic problems have the same solution in the optically thick limit. Furthermore, in the optically thin limit, the heat flux is determined principally by the absorbing/emitting properties of the medium and is not influenced significantly by scattering. Therefore, the scaled isotropic problem can be expected to yield radiative heat fluxes with good precision for all optical thicknesses.

5.3.2. *Eddington approximation.* In the Eddington approximation [26, 27], the radiative intensity $I(\tau,\mu)$ is assumed to be linearly anisotropic. When this approximation is introduced into the radiative transfer equation (18), all terms with $n \geqslant 2$ in the in-scatter integral vanish due to the orthogonality properties of the Legendre polynomials, and thus the full anisotropic scattering problem is effectively reduced to one of linearly anisotropic scattering with phase function $1+a_1\mu\mu'$. Furthermore, the resulting linearly anisotropic scattering problem is scaled exactly using the transformations given by equations (27)–(29).

The Eddington approximation enables simple closed-form expressions to be obtained for the configuration factors. Of particular interest is the combination of configuration factors in equation (26), which is given by

$$\overline{S_1S_2}+\tfrac{1}{2}\overline{DS_2} = \left[\left(\frac{2}{\varepsilon}-1\right)+\frac{\sqrt{3}}{2} \times \frac{\tanh\left((\sqrt{3}/2)\sqrt{(1-\omega^*)}\tau_0^*\right)}{\sqrt{(1-\omega^*)}}\right]^{-1}. \quad (30)$$

5.4. *Numerical results*

The configuration factors have been computed, as described in Section 5.2, for the six droplet clouds with optical thicknesses up to 20 and surface emissivity of 0.1, and compared with the results for isotropic scaling and the Eddington approximation. For the individual configuration factors, $\overline{S_1S_2}$ and $\overline{DS_2}$, the isotropic and Eddington approximations deviate from the 'exact' result by up to 1 and 15%, respectively. These deviations would be significant were it not for the fact that they arise only when the configuration factor is extremely small—at large optical thickness in the case of $\overline{S_1S_2}$ and small optical thickness in the case of $\overline{DS_2}$. In practice, the significant configuration factor is $(\overline{S_1S_2}+\frac{1}{2}\overline{DS_2})$ for which the isotropic and Eddington approximations deviate from the 'exact' result by less than 0.04 and 0.5%, respectively.

The comparison clearly demonstrates that the significant configuration factor for radiative heat transfer through the sodium droplet cloud can be computed with good precision using either the isotropic or the Eddington approximation. In practice, the difference between the numerical results obtained using the two approximations is insignificant. The Eddington approximation has the advantage of yielding a very simple closed-form expression for the configuration factor and for this reason it is used in the present work.

6. APPLICATION OF RESULTS TO FAST REACTOR

For the purposes of illustration, consider heat transfer in a cover gas cavity $2m$ wide. The cover gas is argon. The following conditions and physical properties are used

$$T_1 = 870 \text{ K}$$

$$T_2 = 670 \text{ K}$$

$$\varepsilon = 0.1$$

$$C_p = 525 \text{ J kg}^{-1} \text{ K}^{-1}$$

$$L = 4.2 \text{ MJ kg}^{-1}$$

$$\rho_d = 830 \text{ kg m}^{-3}$$

$$m = \exp(10.5 - 12\,550/T)$$

$$\alpha = 0.007 \text{ kg m}^{-2} \text{ s}^{-1}.$$

The physical properties of sodium were obtained from Sittig [11] and the heat-transfer coefficient was estimated using the Nusselt number correlation for turbulent convective heat transfer between infinite horizontal planes [28]. The limited data on sodium aerosols [2, 3] suggest that the aerosol loading (ratio of aerosol to vapour density) is in the range 0.1–10, corresponding to droplet mass concentrations in the range 3×10^{-4}–3×10^{-2} kg m^{-3}. The corresponding range of optical thicknesses, calculated using the radiative properties derived in Section 3, is 0.6–60 for size distribution 1 and 0.2–20 for size distributions 4–6.

The heat transfer to the roof of the cover gas cavity is calculated from equation (17) with the configuration factor computed from equation (30).

When the cover gas is clear (no sodium droplets in suspension) the total heat flux at the roof is 1.8 kW m^{-2} to which radiation contributes 63% and convection/condensation the remaining 37%.

When the cover gas contains sodium droplets in suspension the total heat flux to the roof is reduced. Figure 3 shows the ratio of the total heat fluxes with and without droplets (that is, the factor by which the total heat flux is reduced due to droplets) as (a) a function of the optical thickness of the droplet cloud, and (b) a function of the mass concentration of droplets in the cloud. The two curves shown in Fig. 3(a) are the extremes for the six droplet clouds. The relatively small spread in the curves indicates that variations in the

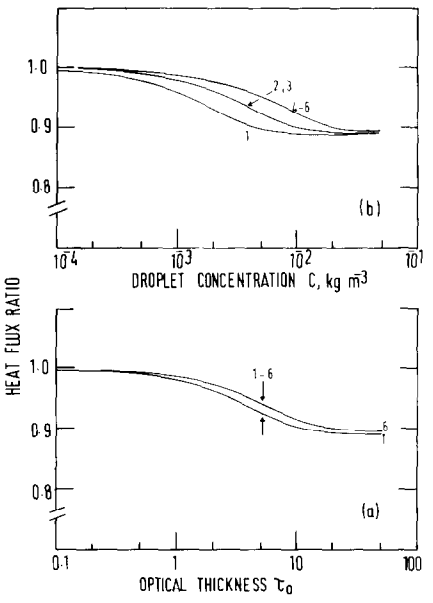

FIG. 3. Ratio of heat fluxes through cover gas with and without droplets in suspension as a function of (a) optical thickness, (b) droplet concentration.

radiative properties of the sodium droplet cloud—albedo and asymmetry—do not sigificantly influence the heat flux. The curves in Fig. 3(b) show the influence of mean droplet size on the heat flux and indicate that, for a fixed mass concentration of droplets, the reduction in the total heat flux is greatest for the cloud with the smallest mean droplet size. It can be seen that the heat flux is reduced by at most 11% due to the presence of the sodium droplets, even when the optical thickness of the droplet cloud becomes large. Only for optical thicknesses greater than about 2—aerosol loadings greater than about 1 in a cavity of width $2m$—is there any appreciable effect of the droplets on heat transfer through the cover gas to the roof.

That the droplets have only a relatively small effect on heat transfer through the cover gas is due to the assumption of a well-mixed, uniform-temperature droplet cloud. Without mixing due to the turbulent convective flow within the cavity, the temperature distribution through the droplet cloud would approach the local-radiative-equilibrium distribution and the radiative heat transfer would be significantly reduced.

To confirm the assumption of uniform temperature in the presence of radiation, the temperature distribution through the medium was calculated from the energy equation for simultaneous turbulent convection and radiation. Turbulent convection was calculated using an eddy heat transport model with prescribed local eddy diffusivity for enthalpy [7] and radiation was calculated using a low order discrete ordinate method (DS_1). The calculated temperature distributions were consistent with the assumption of a uniform temperature core with narrow (optically thin) boundary layers.

7. CONCLUSIONS

The infrared optical constants of sodium predicted using the classical electron theory of metals are in good agreement with the measured data. The radiative properties—absorption and scattering efficiencies and asymmetry—for a polydisperse cloud of sodium droplets depend primarily on the Sauter mean size and only weakly on the shape of the size distribution.

For conditions typical of those encountered in the fast reactor cover gas cavity, the cloud efficiencies for absorption and scattering are essentially independent of wavelength and total (wavelength-averaged) radiative properties can be used in the analysis of radiative heat transfer. The total cloud efficiencies for absorption and scattering are 0.07 and 2.1, respectively, and the single-scatter albedo is 0.97. The total scattering is forward directed and the asymmetry increases slowly with increasing Sauter mean size and is typically in the range 0.2–0.5.

The radiative heat flux through a uniform-temperature cloud of sodium droplets bounded by infinite parallel planes can be calculated with good precision using isotropic scaling and the Eddington approximation. A detailed knowledge of the scattering phase function is not required: the asymmetry is sufficient.

The presence of sodium droplets suspended in the cover gas in a fast reactor is estimated to reduce the total heat flux through the cover gas by less than 10%.

REFERENCES

1. C. F. Clement and P. Hawtin, Transport of sodium through the cover gas of a sodium-cooled fast reactor, Int. Conf. on Liquid Metal Technology in Energy Production (1973) and U.K.A.E.A. report AERE-R7513.
2. B. J. Gliddon and R. C. Hotchkiss, Unpublished work at C.E.G.B. Laboratory, Marchwood, U.K. (1972).
3. *Nuclear Aerosols in Reactor Safety*, Nuclear Energy Agency, OECD (1979).
4. R. J. Goldstein and T. Y. Chu, Thermal convection in a horizontal layer of air, in *Progress in Heat and Mass Transfer* (edited by T. F. Irvine, W. E. Ibele, J. P. Hartnett and R. J. Goldstein), vol. 2, pp. 55–75 (1969).
5. E. F. C. Somerscales and D. Dropkin, Experimental investigation of the temperature distribution in a horizontal layer of fluid heated from below, *Int. J. Heat Mass Transfer* **9**, 1189–1204 (1966).
6. J. W. Elder, The temporal development of a model of high Rayleigh number convection, *J. Fluid Mech.* **35**, 417–437 (1969).
7. F. B. Cheung, Natural convection in a volumetrically heated fluid layer at high Rayleigh number, *Int. J. Heat Mass Transfer* **20**, 499–506 (1977).
8. J. W. Deardorff and G. E. Willis, Investigation of turbulent thermal convection between horizontal plates, *J. Fluid Mech.* **28**, 675–704 (1967).
9. M. Eglème and A. Michel, Sodium entrainment in an argon flow: the evaporation and condensation process, in *Progress in Heat and Mass Transfer* (edited by O. E. Dwyer), vol. 7, pp. 503–516 (1973).
10. F. C. Brown, *The Physics of Solids*. Benjamin, New York (1967).

11. M. Sittig, *Sodium: Its Manufacture, Properties and Uses.* Chapman & Hall, London (1956).
12. H. E. Ives and H. B. Briggs, The optical constants of sodium, *J. Opt. Soc. Am.* **27,** 181 (1937).
13. J. N. Hodgson, The optical effective mass and absorption edge of electrons in sodium, *J. Phys. Chem. Solids* **24,** 1213–1216 (1963).
14. R. Althoff and J. H. Hertz, Measurement of the optical constants of Na and K in the range of wavelength from 2.5 to 10 μ, *Infrared Phys.* **7,** 11–16 (1967).
15. H. C. Van de Hulst, *Light Scattering by Small Particles.* Wiley, New York (1957).
16. G. W. Kattawar and G. N. Plass, Electromagnetic scattering from absorbing spheres, *Appl. Optics* **6,** 1377–1382 (1967).
17. R. A. Dobbins and G. S. Jizmagian, Optical scattering cross-sections for polydispersions of dielectric spheres, *J. Opt. Soc. Am.* **56,** 1345–1350 (1966).
18. R. O. Buckius and D. C. Hwang, Radiation properties for polydispersions: application to coal, *Trans. Am. Soc. Mech. Engrs,* Series C, *J. Heat Transfer* **102,** 99–103 (1980).
19. M. Epstein and D. E. Rosner, Enhancement of diffusion-limited vaporization rates by condensation within the thermal boundary layer: 2. Comparison of homogeneous nucleation theory with critical supersaturation model, *Int. J. Heat Mass Transfer* **13,** 1393–1414 (1970).
20. H. C. Hottel and A. F. Sarofim, *Radiative Transfer.* McGraw-Hill, New York (1967).
21. S. Chandrasekhar, *Radiative Transfer.* Dover, New York (1960).
22. T. J. Love and R. J. Grosh, Radiative heat transfer in absorbing, emitting and scattering media, *Trans. Am. Soc. Mech. Engrs,* Series C, *J. Heat Transfer* **87,** 161–166 (1965).
23. B. Davison, *Neutron Transport Theory.* Oxford University Press, London (1958).
24. H. Lee and R. O. Buckius, Scaling anisotropic scattering in radiation heat transfer for a planar medium, *Trans. Am. Soc. Mech. Engrs,* Series C, *J. Heat Transfer* **104,** 68–75 (1982).
25. K. M. Case and P. F. Zweifel, *Linear Transport Theory.* Addison-Wesley, Reading, Massachusetts (1967).
26. A. S. Eddington, *The Internal Constitution of the Stars.* Dover, New York (1960).
27. R. Viskanta, Radiation transfer and interaction of convection with radiation heat transfer, *Adv. Heat Transfer* **3,** 175–251 (1966).
28. W. H. McAdams, *Heat Transmission.* McGraw-Hill, New York (1954).

TRANSFERT THERMIQUE RADIATIF A TRAVERS UNE COUVERTURE GAZEUSE D'UN REACTEUR RAPIDE REFROIDI AU SODIUM

Résumé—On présente un modèle simple du transfert thermique radiatif à travers la couverture gazeuse d'un réacteur rapide refroidi au sodium. Cette couverture gazeuse est imaginée comme un nuage de gouttelettes de sodium en suspension dans un gaz transparent. Les propriétés radiatives, absorption du nuage de gouttelettes, diffusion, et la fonction de phase de diffusion, sont calculées en utilisant la théorie de Mie de la diffusion électromagnétique avec des propriétés optiques calculées par la théorie électronique classique des métaux. Le transfert radiatif à travers le gaz est calculé rigoureusement en utilisant la méthode de l'ordonnée discrète et comparé avec les résultats obtenus par l'approximation d'Eddington. Des données numériques du modèle sont présentées et utilisées pour estimer l'effet de la diffusion par les gouttelettes sur le transfert thermique à travers la couverture gazeuse d'un réacteur rapide.

STRAHLUNGSWÄRMETRANSPORT DURCH DAS SCHUTZGAS EINES NATRIUMGEKÜHLTEN SCHNELLEN REAKTORS

Zusammenfassung—Es wird ein einfaches Modell des Strahlungswärmetransports durch das Schutzgas eines natriumgekühlten schnellen Reaktors beschrieben. Das Schutzgasmedium wird als eine Wolke von Natrium-Tröpfchen, suspendiert in einem transparenten Gas, angenommen. Die Strahlungseigenschaften der Tröpfchenwolke—Absorption Streuungswirkungsgrad und Streuungsphasenfunktion—werden unter Anwendung der Mie-Theorie der elektromagnetischen Streuung berechnet, wobei die optischen Eigenschaften nach der klassischen Elektronentheorie der Metalle ermittelt werden. Der Strahlungstransport durch das Schutzgas wird streng nach der Methode der diskreten Ordinaten berechnet und mit den Ergebnissen verglichen, die aus den Approximationen der isotropen Skalierung und nach Eddington erhalten wurden. Die numerischen Ergebnisse des Modells werden dargestellt, um damit den Einfluß der Streuung der Tröpfchen auf die Wärmeübertragung durch das Schutzgas des schnellen Reaktors beurteilen zu können.

ЛУЧИСТЫЙ ПЕРЕНОС ТЕПЛА ЧЕРЕЗ ГАЗОВУЮ ОБОЛОЧКУ В БЫСТРОМ РЕАКТОРЕ С НАТРИЕВЫМ ОХЛАЖДЕНИЕМ

Аннотация—Предложена простая модель лучистого переноса тепла через газовую оболочку в быстром реакторе с натриевым охлаждением. Предполагается, что газовая среда состоит из облака капель натрия, взвешенных в прозрачном газе. Лучистые характеристики облака—коэффициенты поглощения и рассеяния и функция фазы рассеяния—рассчитываются по теории Ми для электромагнитного рассеяния с использованием оптических свойств, которые определяются по классической электронной теории металлов. Методом дискретных ординат проведен точный расчет лучистого переноса через газовую оболочку и дано сравнение с результатами, полученными методом изотропного подобия и эддингтоновских аппроксимаций. Представлены численные результаты расчета по описанной модели и с их помощью дана оценка влияния рассеяния на каплях на перенос тепла через газовую оболочку реактора.